Environmental Science & Technology Letters

Letter

pubs.acs.org/journal/estlcu

Loss of Phospholipid Membrane Integrity Induced by Two-Dimensional Nanomaterials

Ines Zucker, Jay R. Werber, Zachary S. Fishman, Sara M. Hashmi, Uri R. Gabinet, Xinglin Lu, Chinedum O. Osuji, Lisa D. Pfefferle, and Menachem Elimelech*

Department of Chemical and Environmental Engineering, Yale University, New Haven, Connecticut 06520-8286, United States

Supporting Information

ABSTRACT: The interaction of two-dimensional (2D) nanomaterials with biological membranes has important implications for ecotoxicity and human health. In this study, we use a dye-leakage assay to quantitatively assess the disruption of a model phospholipid bilayer membrane (i.e., lipid vesicles) by five emerging 2D nanomaterials: graphene oxide (GO), reduced graphene oxide (rGO), molybdenum disulfide (MoS_2), copper oxide (CuO), and iron oxide (α-Fe_2O_3). Leakage of dye from the vesicle inner solution, which indicates loss of membrane integrity, was observed for GO, rGO, and MoS_2 nanosheets but not for CuO and α-Fe_2O_3, implying that 2D morphology by itself is not sufficient to cause loss of membrane integrity. Mixing GO and rGO with lipid vesicles induced aggregation, whereas enhanced stability (dispersion) was observed with MoS_2 nanosheets, suggesting different aggregation mechanisms for the 2D nanomaterials upon interaction with lipid bilayers. No loss of membrane integrity was observed under strong oxidative conditions, indicating that nanosheet-driven membrane disruption stemmed from a physical mechanism rather than chemical oxidation. For GO, the most disruptive nanomaterial, we show that the extent of membrane integrity loss was dependent on total surface area, not edge length, which is consistent with a lipid-extraction mechanism and inconsistent with a piercing mechanism.

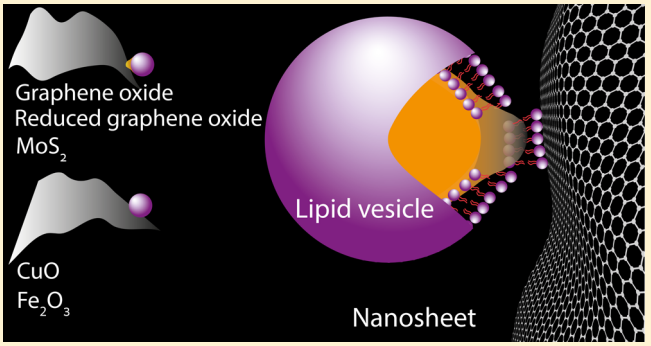

INTRODUCTION

Two-dimensional (2D) nanomaterials are substances with a thickness of a few nanometers or less, resulting in unique and technologically useful properties. The reduced dimensionality of single- to few-layer 2D nanomaterials (i.e., nanosheets) results in high electron mobility, tunable band structures, and high thermal conductivity compared to the characteristics of their bulk material counterparts.[1] These unusual properties have led to an accelerated development of 2D nanomaterial-based products in the electronics, optoelectronics, photonics, and biomedical industries.[2] Not surprisingly, 2D nanomaterials are also attracting extensive interest in environmental science, where applications[3−5] and implications[6,7] of nanosheets are being studied.

The ecotoxicology and environmental impact of 2D nanomaterials strongly depend on interactions with the membrane of living cells, which serves as a barrier between intracellular contents and the surrounding environment.[8−10] Several mechanisms for interaction with cell membranes have been proposed for 2D nanomaterials, including chemical oxidation and physical disruption.[6,7,11] Chemical oxidation can occur either through the generation of reactive oxygen species or through direct electron transfer.[11−15] Physical disruption may be initiated via direct contact with 2D nanomaterials, followed by penetration of the cell membrane.[6,7,13,16,17] Loss of membrane integrity may then propagate through pore formation,[18] adsorption or adhesion to the nanomarial surface,[9,19] or extraction of lipid molecules.[7] This membrane disruption process depends strongly on the availability and orientation of sharp edges as well as the mechanical,[8] morphological,[20] and surface chemical properties of the nanomaterials.[9,16,21]

A comparison between the proposed mechanisms of interaction is difficult, as the characteristics of the tested cell matrix and 2D nanomaterial differed in the various studies. To address the issue of cell complexity, several studies have suggested the use of a simplified model system, such as lipid bilayers, to investigate the critical role of membrane stress during biomolecule−nanomaterial interactions.[8−10] Furthermore, while interaction with cell membranes has been most extensively studied for carbon-based 2D nanomaterials, such as graphene and graphene oxide (GO), very few data are available for other 2D nanomaterials.[2,22] Hence, there is a need to assess and compare the origin of cytotoxicity of emerging 2D nanomaterials.

Received: August 21, 2017
Accepted: September 7, 2017
Published: September 7, 2017

DOI: 10.1021/acs.estlett.7b00358
Environ. Sci. Technol. Lett. XXXX, XXX, XXX−XXX

In this study, we quantitatively assess the disruption of phospholipid vesicles with an entrapped fluorescent dye solution as a surrogate to mimic nanosheet−cell interactions. Five emerging 2D nanomaterials are characterized prior to and during interaction with lipid vesicles, demonstrating different levels of dye leakage (loss of membrane integrity) as well as different aggregation mechanisms. No loss of membrane integrity is observed under highly oxidative conditions, indicating that a physical interaction mechanism rather than chemical oxidation induces lipid membrane disruption by the nanosheets. Additionally, the physical interaction of the most disruptive nanomaterial (GO) and lipid vesicles is found to be dependent on the surface area rather than the edge. The findings of this study provide new experimental insights into the mechanisms of interaction of nanosheets with lipid bilayers, with implications for the interaction of nanosheets with real cell membranes.

MATERIALS AND METHODS

Two-Dimensional Materials. GO nanosheets were received as an aqueous suspension (6.2 g/L) from a commercial source (Graphene Supermarket). Different GO sheet area distributions were obtained by probe sonication[20] of the GO suspension (1 g/L) for 0, 1, 10, and 30 min at high intensity (6.5 kW/L, Misonix 3000, Misonix Inc., Farmingdale, NY) while the sample was being cooled in an ice bath to prevent an increase in temperature during the sonication process. Reduced GO nanosheets were produced under mild conditions[23] using L-ascorbic acid (L-AA, Sigma). Specifically, 15 mg of L-AA was added to 15 mL of a diluted aqueous suspension of GO (1 mg/mL) under vigorous stirring at room temperature for 4 h.

A chemically exfoliated molybdenum disulfide (MoS_2) nanosheet suspension was synthesized through Li intercalation[24] and used within 4 days of preparation. Cupric oxide (CuO) nanosheets were synthesized via a surfactant-assisted aqueous-phase method,[25] while hematite (α-Fe_2O_3) nanosheets were grown using CuO nanosheets as a hard template by adding iron(II) sulfate heptahydrate.[26] A detailed description of the synthesis methods for MoS_2, CuO, and α-Fe_2O_3 nanosheets can be found in the Supporting Information. CuO and α-Fe_2O_3 nanosheet powders were suspended in deionized water prior to experiments. All nanosheet suspensions were bath-sonicated for 10 min (26 W/L, FS60 Ultrasonic Cleaner) immediately prior to characterization and interaction with lipid vesicles.

Characterization of Materials. GO, rGO, MoS_2, CuO, and α-Fe_2O_3 nanosheets were comprehensively characterized using transmission electron microscopy (TEM) for nanostructure morphology; atomic force microscopy (AFM) for nanosheet thickness; the Brunauer, Emmett, and Teller (BET) method for dry surface area; dynamic light scattering (DLS) and static light scattering (SLS) for dispersed aggregate size (presented as diffusive time, or τ, in milliseconds and corresponding hydrodynamic radius in nanometers) and morphology; ζ potential for surface charge in biological media; and contact angle for hydrophilicity. Further details of the characterization methods and sample preparation can be found in the Supporting Information.

Preparation of Lipid Bilayer Vesicles. Lipid vesicles were prepared via the film rehydration method.[27] Monounsaturated synthetic lipid 1,2-dioleoyl-*sn*-glycero-3-phosphocholine (DOPC, Avanti Polar Lipids) (10 mg) in chloroform was dried in a glass tube under a stream of nitrogen gas to form a thin film. The DOPC film was placed under vacuum overnight to remove residual chloroform. The dried film was subsequently rehydrated with agitation in MOPS buffer (pH 7.5, 50 mM NaMOPS) with 50 mM 5(6)-carboxyfluorescein (CF, Acros) to form multilamellar vesicles. Extrusion through a polycarbonate track-etch membrane with a 100 nm pore size (GE Whatman) using a miniextruder 21 times (Avanti Polar Lipids) enabled the formation of unilamellar vesicles. The lipid vesicle solution was passed through a HiTrap desalting column (GE Healthcare Life Sciences) equilibrated with biological buffer [50 mM MOPS and 90 mM NaCl (pH 7.5)] to remove CF that was not encapsulated by the lipid vesicles. The prepared vesicle stock solution had a DOPC concentration of 4 mg/mL and vesicles with an average hydrodynamic diameter of 140 nm, as determined by DLS. The stock solution was used the day it was prepared.

Dye-Leakage Assay. Dye-leakage experiments were performed by placing dye-encapsulated lipid vesicles in contact with suspended nanosheets. The vesicle stock solution was diluted using a biological buffer [50 mM MOPS and 90 mM NaCl (pH 7.5)] to obtain a DOPC concentration of 100 mg/L. The vesicle solution exhibited a low background fluorescence intensity because of the self-quenching of fluorescence for CF dye at a high concentration (above ~10 mM).[28] Nanosheets were added to a final concentration of 5 mg/L to initiate interaction with the vesicles. Fluorescence was monitored continually for the first 45 min and following interaction for 1, 2, or 3 h using a spectrofluorometer (Synergy HT, Bio-Tek) at excitation and emission wavelengths of 485 and 528 nm, respectively. The normalized fraction of leaked CF was calculated using

$$\frac{C}{C_{max}} = \frac{I - I_0}{I_{max} - I_0} \tag{1}$$

where C is the CF concentration at a specific time interval, I is the measured fluorescence intensity at a specific time interval, and I_0 is the initial fluorescence intensity before the exposure. A non-ionic surfactant (Triton X-100) was added at a concentration of 0.5 wt %, solubilizing the lipid vesicles and releasing all entrapped fluorophore, to determine the total measured fluorescence intensity, I_{max}, and maximum CF dye concentration, C_{max}. Experiments were also conducted to assess the effect of oxidative conditions and dye adsorption by nanomaterials, as described in the Supporting Information.

A kinetic model was developed to gain insight into the underlying interaction mechanisms of lipid vesicles with the different nanosheets. Model development assumed a second-order interaction, with nanosheets and vesicles as the two "reactants", and is described in detail in the Supporting Information. The final equation for the decrease in vesicle integrity is given as

$$\frac{N}{N_0} = \frac{\frac{N_f}{N_0}}{1 - \left(1 - \frac{N_f}{N_0}\right)\exp(-k_1 k_2 N_f t)} \tag{2}$$

where N/N_0 is the relative concentration of undisrupted (i.e., dye-filled) lipid vesicles, N_0 and N_f are the initial and final concentrations of undisrupted vesicles, respectively, k_1 is the rate constant for the interaction between vesicles and nanosheets, and k_2 is the proportionality constant between the number of available nanosheet reactive sites and the concentration of undisrupted vesicles.

DOI: 10.1021/acs.estlett.7b00358
Environ. Sci. Technol. Lett. XXXX, XXX, XXX−XXX

Table 1. Key Material Properties of the 2D Nanomaterials Used in This Study

	approximate size (dry) (nm) (TEM)	nanosheet thickness (dry) (nm) (AFM)	specific surface area (dry) (m^2/g) (BET)	dispersed aggregate size: DLS τ[a] (ms)	dispersed aggregate size: DLS size[b] (PDI)[c] (nm, −)	dispersed aggregate morphology (fractal dimension, D_f) (SLS)	ζ potential in biological media (mV) (Zetasizer)	hydrophilicity (deg) (water contact angle)
GO	200−3000	0.8−1.5	490.0	4.27	1013 (0.14)	2.19	−25.6 ± 0.8	18 ± 3
rGO	200−3000	3.0−3.5	<37.4[d]	4.69	1130 (0.06)	2.22	−27.8 ± 1.0	58 ± 10
MoS_2	200−600	3.0−5.0	17.8	0.85−2.28[e]	180−550[e]	2.51	−33.2 ± 1.1	65 ± 7
CuO	200−3000	7.0−15.0	23.0	4.19	1009 (0.05)	2.08	−6.8 ± 1.5	<10
α-Fe_2O_3	200−3000	5.0−10.0	139.0	5.09	1227 (0.06)	2.50	+5.1 ± 0.9	<10

[a]Dynamic light scattering presented as diffusive time. [b]Dynamic light scattering presented as the corresponding spherical hydrodynamic radius (averaged over a 1 h data collection period). [c]Polydispersity index. [d]The adsorption isotherm for rGO was inconsistent, possibly because of the small surface area induced by aggregation during the reduction process and/or the outgassing heat treatment. [e]Size range of MoS_2 nanosheets grown during a 1 h data collection period (see Figure 2).

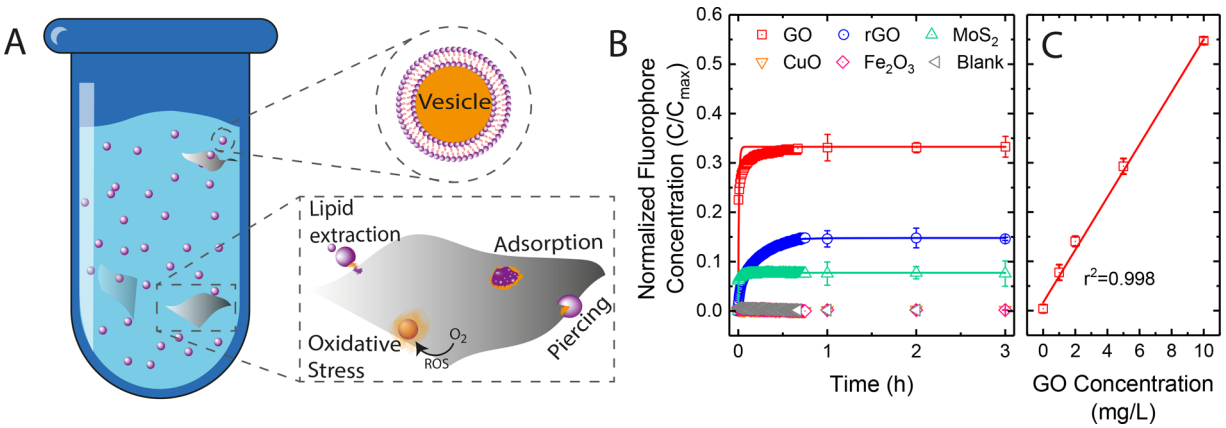

Figure 1. (A) Schematic illustrating the experimental setup, lipid vesicle structure encapsulating a fluorescent dye at high concentration, and possible mechanisms of interaction between nanosheets and vesicles. (B) Kinetics of leakage of the fluorescent dye from a vesicle (100 mg/L) inner solution to the extravesicular solution induced by two-dimensional nanomaterials (5 mg/L), including fitting to eq 2. (C) Correlation between fluorophore release and graphene oxide (GO) nanosheet concentration after 1 h of interaction.

RESULTS AND DISCUSSION

Material-Dependent Loss of Membrane Integrity. Relevant characteristics of the 2D nanomaterials such as size, morphology, surface area, surface charge, and hydrophilicity (indicated by contact angle) are presented in Table 1 and Figures S1−S4. To study the effects of nanosheets on membrane integrity, suspended 2D nanomaterials were contacted with phospholipid vesicles encapsulating a high concentration of self-quenching CF fluorophore, as illustrated in Figure 1A. The leakage of the fluorescent solution into the extravesicular solution because of membrane damage eliminated self-quenching and led to a linear increase in fluorescence over the range of interest [0−15 μM (Figure S5)].

Figure 1B presents the change in fluorophore concentration in the extravesicular solution with interaction time. The blank solution (lipid vesicles in a buffer solution) showed a minimal increase in extravesicular fluorophore concentration, indicating that the lipid bilayer is impermeable to the charged fluorescent dye at the time scales investigated. A negligible increase in extravesicular fluorophore concentration was also observed in the presence of CuO and α-Fe_2O_3 nanosheets, implying that these nanosheets did not compromise membrane integrity under our experimental conditions. The limited interaction of the two metal oxide nanosheets with lipid vesicles can be partially attributed to their instability in solution and tendency to settle, as supported by ζ potential and continuous DLS measurements (Table 1 and Figure S3, respectively).

In contrast, vesicle solutions mixed with GO, rGO, and MoS_2 nanosheets showed a rapid and significant increase in extravesicular fluorophore concentration. Interaction of lipid vesicles with GO nanosheets resulted in the highest degree of fluorophore leakage (33 ± 3%) after contact for 3 h, followed by rGO (15 ± 2%) and MoS_2 (8 ± 2%). Additionally, an increased GO nanosheet concentration resulted in a linear increase in the rate of fluorophore release (Figure 1C), indicating that reactive sites on the nanosheets are consumed during the interaction, as opposed to catalyzing further fluorophore release. We note that adsorption of dye to the nanomaterials was found to negligibly affect our results (Figure S6).

A greater loss of membrane integrity in the presence of GO compared to that in the presence of rGO can be interpreted using previously published results with model bacteria. Akhaven et al.[16] suggested an increased level of damage of Gram-negative bacteria following reduction of GO nanowalls deposited on stainless steel substrates, which was attributed to the edge properties of the reduced nanowalls (sharper and greater charge transfer). However, GO suspensions showed antibacterial activity for Gram-negative bacteria greater than that of rGO,[13] similar to our observed trends in a loss of phospholipid membrane integrity. It was suggested that different interactions occur for GO and rGO; while GO thin layers can wrap cells,[29,30] cells might be embedded in large rGO aggregates.[13] Aggregation of rGO nanosheets was also

DOI: 10.1021/acs.estlett.7b00358
Environ. Sci. Technol. Lett. XXXX, XXX, XXX−XXX

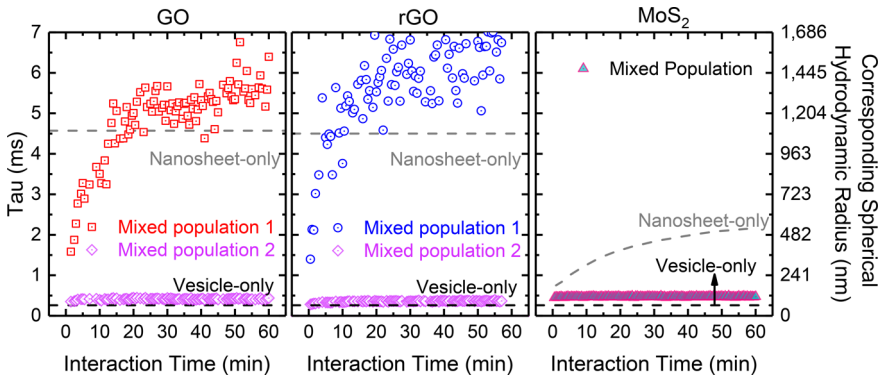

Figure 2. Aggregation kinetics for graphene oxide (GO), reduced graphene oxide (rGO), and molybdenum disulfide (MoS_2) nanosheets (5 mg/L) with lipid vesicles (100 mg/L) as determined by dynamic light scattering. Dashed lines represent control measurements for vesicle solutions and for GO, rGO, and MoS_2 nanosheet suspensions. Light scattering data are presented as τ (diffusive time, left vertical axis) and the corresponding spherical hydrodynamic radius (right vertical axis). Two populations (mixed populations 1 and 2) appear for GO and rGO during interaction with lipid vesicles, while one population is observed for MoS_2 when mixed with lipid vesicles.

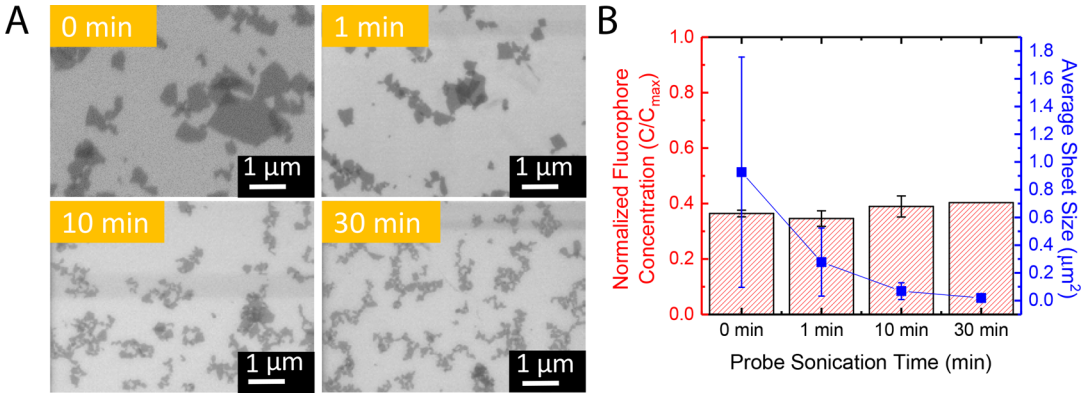

Figure 3. Surface area-dependent interaction of nanosheets and lipid vesicles. (A) Representative scanning electron microscopy (SEM) images of probe-sonicated GO nanosheets drop cast onto a silicon wafer. A GO suspension (1 g/L) was probe-sonicated for 0, 1, 10, and 30 min at a high power density (6.5 kW/L) while the sample was cooled in an ice bath to prevent an increase in temperature during sonication. (B) Release of dye from lipid vesicles (100 mg/L) induced by probe-sonicated GO nanosheets (5 mg/L). The sheet size (expressed as area) was measured for at least 50 GO sheets from SEM images using ImageJ.

evidenced in our study by an approximately 10-fold decrease in the specific surface area and a corresponding increase in nanosheet thickness (Table 1).

Kinetic models were applied to the data presented in Figure 1B to gain insight into potential differences in the underlying mechanisms of interaction of lipid vesicles with the different nanosheets. Experimental results of dye leakage induced by rGO and MoS_2 agreed well with the second-order kinetic model (eq 2); however, modeled dye leakage induced by GO was overestimated at the initial stage of interaction (<45 min). This result suggests that the interaction of GO with lipid vesicles has kinetics different from those of a simple second-order interaction.

Aggregation Mechanisms Differ between Two-Dimensional Materials. To further investigate the association of 2D nanomaterials with lipid vesicles, the aggregation and dispersion characteristics of nanosheets and vesicles as well as changes in aggregate size during interaction were determined by continuous DLS measurements (Figure 2). Because of the complexity of the mixed system with particles of different shapes (i.e., spherelike vesicles and sheetlike 2D nanomaterials), the change in aggregate size is represented here by the change in the diffusive time (τ), with a greater diffusive time indicating a larger particle size. Control experiments (i.e., nanosheets with no vesicles) showed that GO and rGO nanosheet sizes were stable through the entire experiment and had similar diffusive times (i.e., similar size). The MoS_2 nanosheet size increased with time because of spontaneous aggregation, indicating that MoS_2 nanosheets are not stable in an aqueous suspension.[31] Vesicle size was constant throughout the experiment and had diffusive times similar to those of MoS_2 nanosheets, implying that they are roughly similar in size (~140−200 nm).

To evaluate the aggregation mechanism during exposure of lipid vesicles (100 mg/L) to nanosheets (5 mg/L), light scattering data were collected for 1 h immediately after mixing. Two size populations were found (simultaneously) during the interaction of GO and rGO with lipid vesicles. The observed stable population was attributed to undisrupted lipid vesicles (tracing the "vesicle-only" control line), while the second population grew in size with time (to a size even greater than the nanosheet control), indicating that aggregation was induced by the interaction of GO and rGO with lipid vesicles. Similar formation of mixed aggregates was observed following interaction of GO with bacteria and fungal spores.[30]

Only one population was found during the interaction of MoS_2 with vesicles, because of their similar initial sizes. In contrast to the graphene-based materials, aggregate size did not

DOI: 10.1021/acs.estlett.7b00358
Environ. Sci. Technol. Lett. XXXX, XXX, XXX−XXX

change with time, indicating stabilization of MoS_2 nanosheets induced by lipid vesicles. The stabilization of MoS_2 versus aggregation of GO and rGO when mixed with lipid vesicles suggests that, while each nanosheet material physically interacts with the lipid vesicles, different interactions that depend on the chemical composition and physicochemical characteristics of the given nanosheet occur.

Surface Area-Dependent Physical Interaction between GO and Lipid Bilayer Vesicles. Proposed mechanisms for disruption of biological membranes by nanosheets include chemical and physical interactions. The primary chemical mechanism is oxidative stress.[15] The effect of oxidative conditions on the membrane integrity of lipid vesicles was evaluated in the presence of moderately reactive (H_2O_2) and highly reactive (hydroxyl radicals produced by H_2O_2 and ultraviolet irradiation) oxidant species. We found a negligible effect on membrane integrity in the presence of the oxidants (Figure S7), while the inner fluorophore solution was chemically degraded by hydroxyl radicals. This finding suggests that our observed fluorophore leakage during interaction with 2D nanomaterials is due to physical membrane perturbation by nanosheets.

For carbon-based nanosheets, model simulations proposed two physical interaction mechanisms: (i) lipid extraction leading to the adsorption of lipids to the nanosheet surface (i.e., surface area-dependent physical interaction)[7] and (ii) a piercing mechanism forming pores in the cell membrane bilayer (i.e., edge-dependent physical interaction).[18] To improve our understanding of the predominant mechanism, the GO suspension (our most disruptive 2D nanomaterial) was probe-sonicated for increasing times prior to interaction with vesicles. After sonication, the total surface area of the GO suspension remained constant, while the total edge length increased because of breakage of GO into smaller nanosheets. Scanning electron microscopy (SEM) imaging demonstrated the decrease in nanosheet size (area) with sonication time for a 1 g/L GO suspension (Figure 3A), which directly indicates an increase in edge density. Figure 3B demonstrates the loss of vesicle integrity induced by probe-sonicated GO nanosheets (5 mg/L). An increased edge density had no effect on dye leakage, suggesting that a surface area-dependent physical interaction is the predominant mechanism, rather than an edge-dependent mechanism.

The results depicted in Figure 3, together with the observed asymptotic behavior in Figure 1B indicating consumption of active sites on the membrane-disrupting nanosheets, support a mechanism of destructive extraction of phospholipids from cell membranes,[7] as this mechanism would be limited by the surface area available for lipid adsorption. In contrast, the results are inconsistent with pore formation via a piercing mechanism, which should increase with edge density.[9,18] However, we note that penetration via sheet edges might be necessary to initiate the interaction and expose the hydrophobic inner region of the membrane.[6,7] The surface area-dependent physical interaction emphasizes the finding that the stability and surface functionality of nanosheets may play an important role in interaction with cells. Furthermore, no correlation was found between the edge density of the different nanosheet types (GO, rGO, and MoS_2) and fluorophore release, while the surface area concentration loosely correlated with the loss of cell membrane integrity (Figure S8). Overall, although we have used simplified membranes that lack the complexity of real cell membranes,[32] lessons learned from our study may provide meaningful insights into potential interactions of 2D nanosheets with living cells.

■ ASSOCIATED CONTENT

Supporting Information

The Supporting Information is available free of charge on the ACS Publications website at DOI: 10.1021/acs.estlett.7b00358.

Methodology for synthesis of nanosheets, methodology for material characterization, kinetic model development, oxidative conditions, and dye adsorption by nanomaterials and supporting figures, including representative TEM images of the 2D nanomaterials (Figure S1), representative AFM images of the nanosheets (Figure S2), dynamic light scattering analysis of nanosheet suspensions (Figure S3), ultraviolet−visible spectra of a graphene oxide aqueous suspension before and after reduction (Figure S4), the linear increase in fluorescence for free carboxyfluorescein (Figure S5), the change in fluorescence due to adsorption by nanosheets (Figure S6), the limited role of oxidative conditions in the disruption rate of vesicles (Figure S7), and the correlation between material physical characteristics and damage to lipid vesicles (Figure S8) (PDF)

■ AUTHOR INFORMATION

Corresponding Author

*P.O. Box 208286, Yale University, New Haven, CT 06520. E-mail: menachem.elimelech@yale.edu. Phone: +1 (203) 432-2789. Fax: +1 (203) 432-2881.

ORCID

Ines Zucker: 0000-0001-7408-6757
Xinglin Lu: 0000-0002-0229-7712
Chinedum O. Osuji: 0000-0003-0261-3065
Menachem Elimelech: 0000-0003-4186-1563

Notes

The authors declare no competing financial interest.

■ ACKNOWLEDGMENTS

The authors acknowledge the support received from the National Science Foundation through the Engineering Recearch Center for Nanotechnology Enabled Water Treatment (ERC-1449500). We also acknowledge the YIBS Postdoctoral Fellowship and Tel Aviv University Presidential Postdoctoral Fellowship awarded to I.Z. Z.F. and L.P. acknowledge support from the Army Research Laboratory (QRO grant #64935, Agreement W911NF1410564). Facilities use was supported by the Facility for Light Scattering and YINQE with great help from Dr. Michael Rooks. The authors thank Gilad Kaufman, Camrynn Fausey, and Ben Zucker for their advice and help with data analysis.

■ REFERENCES

(1) Butler, S. Z.; Hollen, S. M.; Cao, L.; Cui, Y.; Gupta, J. A.; Gutierrez, H. R.; Heinz, T. F.; Hong, S. S.; Huang, J.; Ismach, A. F.; Johnston-Halperin, E.; Kuno, M.; Plashnitsa, V. V.; Robinson, R. D.; Ruoff, R. S.; Salahuddin, S.; Shan, J.; Shi, L.; Spencer, M. G.; Terrones, M.; Windl, W.; Goldberger, J. E. Progress, challenges, and opportunities in two-dimensional materials beyond graphene. *ACS Nano* **2013**, 7 (4), 2898−2926.

(2) Ferrari, A. C.; et al. Science and technology roadmap for graphene, related two-dimensional crystals, and hybrid systems. *Nanoscale* **2015**, 7 (11), 4598−4810.

DOI: 10.1021/acs.estlett.7b00358
Environ. Sci. Technol. Lett. XXXX, XXX, XXX−XXX

(3) Yang, W.; Ratinac, K. R.; Ringer, S. P.; Thordarson, P.; Gooding, J. J.; Braet, F. Carbon nanomaterials in biosensors: should you use nanotubes or graphene? *Angew. Chem., Int. Ed.* **2010**, *49* (12), 2114−2138.
(4) He, Q.; Wu, S.; Yin, Z.; Zhang, H. Graphene-based electronic sensors. *Chem. Sci.* **2012**, *3* (6), 1764−1772.
(5) Abraham, J.; Vasu, K. S.; Williams, C. D.; Gopinadhan, K.; Su, Y.; Cherian, C. T.; Dix, J.; Prestat, E.; Haigh, S. J.; Grigorieva, I. V.; Carbone, P.; Geim, A. K.; Nair, R. R. Tunable sieving of ions using graphene oxide membranes. *Nat. Nanotechnol.* **2017**, *12* (6), 546−550.
(6) Li, Y.; Yuan, H.; von dem Bussche, A.; Creighton, M.; Hurt, R. H.; Kane, A. B.; Gao, H. Graphene microsheets enter cells through spontaneous membrane penetration at edge asperities and corner sites. *Proc. Natl. Acad. Sci. U. S. A.* **2013**, *110* (30), 12295−12300.
(7) Tu, Y. S.; Lv, M.; Xiu, P.; Huynh, T.; Zhang, M.; Castelli, M.; Liu, Z. R.; Huang, Q.; Fan, C. H.; Fang, H. P.; Zhou, R. H. Destructive extraction of phospholipids from Escherichia coli membranes by graphene nanosheets. *Nat. Nanotechnol.* **2013**, *8* (8), 594−601.
(8) Hirano, A.; Uda, K.; Maeda, Y.; Akasaka, T.; Shiraki, K. One-dimensional protein-based nanoparticles induce lipid bilayer disruption: Carbon nanotube conjugates and amyloid fibrils. *Langmuir* **2010**, *26* (22), 17256−17259.
(9) Moghadam, B. Y.; Hou, W. C.; Corredor, C.; Westerhoff, P.; Posner, J. D. Role of nanoparticle surface functionality in the disruption of model cell membranes. *Langmuir* **2012**, *28* (47), 16318−16326.
(10) Liu, X.; Chen, K. L. Interactions of graphene oxide with model cell membranes: Probing nanoparticle attachment and lipid bilayer disruption. *Langmuir* **2015**, *31* (44), 12076−12086.
(11) Yang, X.; Li, J.; Liang, T.; Ma, C.; Zhang, Y.; Chen, H.; Hanagata, N.; Su, H.; Xu, M. Antibacterial activity of two-dimensional MoS2 sheets. *Nanoscale* **2014**, *6* (17), 10126−10133.
(12) Romero-Vargas Castrillón, S.; Perreault, F.; De Faria, A. F.; Elimelech, M. Interaction of graphene oxide with bacterial cell membranes: Insights from force spectroscopy. *Environ. Sci. Technol. Lett.* **2015**, *2* (4), 112−117.
(13) Liu, S.; Zeng, T. H.; Hofmann, M.; Burcombe, E.; Wei, J.; Jiang, R.; Kong, J.; Chen, Y. Antibacterial activity of graphite, graphite oxide, graphene oxide, and reduced graphene oxide: Membrane and oxidative stress. *ACS Nano* **2011**, *5* (9), 6971−6980.
(14) Gurunathan, S.; Woong Han, J.; Abdal Daye, A.; Eppakayala, V.; Kim, J. Oxidative stress-mediated antibacterial activity of graphene oxide and reduced graphene oxide in Pseudomonas aeruginosa. *Int. J. Nanomed.* **2012**, *7*, 5901−5914.
(15) Liu, X.; Sen, S.; Liu, J.; Kulaots, I.; Geohegan, D.; Kane, A.; Puretzky, A. A.; Rouleau, C. M.; More, K. L.; Palmore, G. T. R.; Hurt, R. H. Antioxidant deactivation on graphenic nanocarbon surfaces. *Small* **2011**, *7* (19), 2775−2785.
(16) Akhavan, O.; Ghaderi, E. Toxicity of graphene and graphene oxide nanowalls against bacteria. *ACS Nano* **2010**, *4* (10), 5731−5736.
(17) Hui, L.; Piao, J. G.; Auletta, J.; Hu, K.; Zhu, Y.; Meyer, T.; Liu, H.; Yang, L. Availability of the basal planes of graphene oxide determines whether it is antibacterial. *ACS Appl. Mater. Interfaces* **2014**, *6* (15), 13183−13190.
(18) Pham, V. T. H.; Truong, V. K.; Quinn, M. D. J.; Notley, S. M.; Guo, Y.; Baulin, V. A.; Al Kobaisi, M.; Crawford, R. J.; Ivanova, E. P. Graphene induces formation of pores that kill spherical and rod-shaped bacteria. *ACS Nano* **2015**, *9* (8), 8458−8467.
(19) Perreault, F.; Fonseca de Faria, A.; Elimelech, M. Environmental applications of graphene-based nanomaterials. *Chem. Soc. Rev.* **2015**, *44* (16), 5861−5896.
(20) Perreault, F.; De Faria, A. F.; Nejati, S.; Elimelech, M. Antimicrobial properties of graphene oxide nanosheets: Why size matters. *ACS Nano* **2015**, *9* (7), 7226−7236.
(21) Gilbertson, L. M.; Albalghiti, E. M.; Fishman, Z. S.; Perreault, F.; Corredor, C.; Posner, J. D.; Elimelech, M.; Pfefferle, L. D.; Zimmerman, J. B. Shape-dependent surface reactivity and antimicrobial activity of nano-cupric oxide. *Environ. Sci. Technol.* **2016**, *50* (7), 3975−3984.
(22) Wang, Z.; Zhu, W.; Qiu, Y.; Yi, X.; von dem Bussche, A.; Kane, A.; Gao, H.; Koski, K.; Hurt, R. Biological and environmental interactions of emerging two-dimensional nanomaterials. *Chem. Soc. Rev.* **2016**, *45* (6), 1750−1780.
(23) Zhang, J.; Yang, H.; Shen, G.; Cheng, P.; Zhang, J.; Guo, S. Reduction of graphene oxide via L-ascorbic acid. *Chem. Commun.* **2010**, *46* (7), 1112−1114.
(24) Joensen, P.; Frindt, R. F.; Morrison, S. R. Single-layer MoS2. *Mater. Res. Bull.* **1986**, *21* (4), 457−461.
(25) Fishman, Z. S.; Rudshteyn, B.; He, Y.; Liu, B.; Chaudhuri, S.; Askerka, M.; Haller, G. L.; Batista, V. S.; Pfefferle, L. D. Fundamental role of oxygen stoichiometry in controlling the band gap and reactivity of cupric oxide nanosheets. *J. Am. Chem. Soc.* **2016**, *138* (34), 10978−10985.
(26) Fishman, Z.; He, Y.; Yang, K.; Lounsbury, A.; Zhu, J.; Tran, T.; Zimmerman, J.; Batista, V. S.; Pfefferle, L. Hard templating ultrathin polycrystalline hematite nanosheets: effect of nano-dimension on CO_2 to CO conversion via the reverse water-gas shift reaction. *Nanoscale* **2017**, n/a.
(27) Zhang, H. Thin-film hydration followed by extrusion method for liposome preparation. In *Liposomes: Methods and Protocols*; D'Souza, G. G. M., Ed.; Springer: New York, 2017; pp 17−22.
(28) Weinstein, J. N.; Blumenthal, R.; Klausner, R. D. Carboxyfluorescein leakage assay for lipoprotein-liposome interaction. In *Methods in Enzymology*; Ziegler, C., Ed.; Elsevier: Amsterdam, 1986; pp 657−668.
(29) Liu, S.; Hu, M.; Zeng, T. H.; Wu, R.; Jiang, R.; Wei, J.; Wang, L.; Kong, J.; Chen, Y. Lateral dimension dependent antibacterial activity of graphene oxide sheets. *Langmuir* **2012**, *28* (33), 12364−12372.
(30) Chen, J.; Peng, H.; Wang, X.; Shao, F.; Yuan, Z.; Han, H. Graphene oxide exhibits broad-spectrum antimicrobial activity against bacterial phytopathogens and fungal conidia by intertwining and membrane perturbation. *Nanoscale* **2014**, *6* (3), 1879−1889.
(31) Divigalpitiya, W. M. R.; Frindt, R. F.; Morrison, S. R. Inclusion systems of organic molecules in restacked single-layer molybdenum disulfide. *Science* **1989**, *246* (4928), 369−371.
(32) Chen, K. L.; Bothun, G. D. Nanoparticles meet cell membranes: Probing nonspecific interactions using model membranes. *Environ. Sci. Technol.* **2014**, *48* (2), 873−880.

DOI: 10.1021/acs.estlett.7b00358
Environ. Sci. Technol. Lett. XXXX, XXX, XXX−XXX